Impact of Soft Magnetic Material on Design of High Speed Permanent Magnet Machines

Nuwantha Fernando, *Member*, *IEEE*, Gaurang Vakil, Puvan Arumugam,*Member*, *IEEE*, Emmanuel Amankwah, Chris Gerada, *Member*, *IEEE*, and Serhiy Bozhko, *Member*, *IEEE*

***Abstract*—This paper investigates the effect of two soft magnetic materials on a high speed machine design, namely 6.5% Silicon Steel and Cobalt-Iron alloy. The effect of design parameters on the machine performance as an aircraft starter-generator is analysed. The material properties which include B-H characteristics and the losses are obtained at different frequencies under an experiment and used to predict the machine performance accurately. In the investigation presented in this paper, it is shown that machines designed with 6.5% Silicon Steel at a high core flux density has lower weight and lower losses than the Cobalt-Iron alloy designs. This is mainly due to the extra weight contributed by the copper content especially in the end-windings. Due to the high operating frequencies, the core-losses in the Cobalt-Iron machine designs are found to outweigh the copper-losses incurred in the Silicon Steel machines. It is also shown that change in stack length/number of turns has a considerable effect on the copper losses at starting, however has no significant advantage on rated efficiency which happens to be in a field-weakening operating point. It is also shown that the performance of the machine designs depend significantly on material selection and the operating point of the core. The implications of the variation of design parameters on the machine performance is discussed and provides insight into the influence of parameters that effect overall power density.**

***Index Terms*—Aircraft, cobalt steel, flux density, high speed, machine design, soft magnetic material, silicon steel**

I. Introduction

DUE to the increase in per-capita energy demand on-board aircraft and the associated weight penalty of power generation systems on the aircraft fuel consumption, the development of energy efficient aircraft generation systems are progressing rapidly [1]–[4]. One approach that may increase the power generation capability with low weight is to consider machines that operate at high speeds [5]–[14]. This result in increased losses in both the winding material and magnetic material due to high frequencies [15]. Minimizing these losses allows improvement of the design efficiency.

In general, electrical machines associated with aerospace and defence applications tend to employ Cobalt-Iron (Co-Iron) alloy material [16]. This is mainly due to the high temperature operating conditions often encountered in such application and especially high flux density capability of the Co-Iron alloy material which may allow weight minimization. In contrast, Silicon-Iron alloys and sintered soft magnetic materials are also extensively used in automotive [17]–[20] and industrial drive applications [21]–[23] due to their low losses. The sintered soft magnetic material is found to offer relatively poor structural characteristics whilst Silicon-Iron alloys provide increased tensile strength due to alloying high Silicon (Si) content with Iron (Fe).

Different grades of Silicon Steel (Si-Steel) have been researched for machine design in the recent past. The authors of [24] compare grain oriented Si-Steel 35Q145 and non-grain oriented Si-Steel 35WW250 for an axial flux switched reluctance motor design. It is shown in [24] that by appropriate design with the grain oriented Si-Steel material, the efficiency can be improved by 20%. In [25] a high speed, low power PM motor is developed with an amorphous alloy Metglas-2605 soft magnetic core. The research does not present any comparison with alternative material. However, the efficiency of the motor is shown to have reached 90%. The authors of [26] investigate the effect of a thin non-oriented 3% Si-Steel material NO20 in comparison with conventional non-oriented Si-Steel grades M600-100A, M400-50A and M330P-50A. It is shown that M330P-50A based design achieves the highest power density while NO20 achieves highest efficiency. However, in [26] the considered operation is limited to 6000 rpm and does not consider the impact of high speed operation.

Recently, steel with high Si content (6.5% Si-Steel) has been introduced in the market. In contrast with conventional electrical steel with 3% to 4% Si content, the high Si content allows reduction of the electric resistivity of the material and also magnetostriction [27] (length change on magnetization). This further benefit in the reduction of the iron losses associated with machines operating at high speeds. The authors of [28] develop a rare-earth free switched reluctance motor with the use of 6.5% Si-Steel. [28] also compares the machine performance with a conventional low-loss Si-Steel 35A300 and shows that the developed motor achieves a core-loss 25% of that of a 35A300 steel based design. Comparable performance to an interior-permanent magnet synchronous machine

Manuscript received December 27, 2015; revised March 28, 2016 and April 28, 2016; accepted May 9, 2016. This work was funded under the 7th FWP (Seventh Framework Programme) Joint Technology Initiatives - theme Clean Sky. Project Code: JTI-CS-2011-1-ECO-02-009 Alternator with active power rectification and health monitoring

The corresponding author is Puvan Arumugam who is currently with Force Engineering Ltd, Shepshed, UK (email: puvan@force.co.uk)

Nuwantha Fernando is currently with the RMIT University, Melbourne Australia. (email: nuwantha.fernando@rmit.edu.au)

G. Vakil, E Amankwah, C. Gerada and S. Bozhko are with the Power Electronics, Machines and Control Group, Faculty of Engineering, The University of Nottingham, University Park, Nottingham NG7 2RD, U.K.

(IPMSM) is shown at majority of operating conditions expect at high torque conditions. The authors of [29] present the enhancement of efficiency of high speed switched reluctance motors designed with Hiperco-50 (Cobalt-Iron alloy) and with conventional non-oriented Si-Steel 35A300. It is shown that a Co-Iron based switched reluctance machine achieves higher efficiency compared with a Si-Steel based design. The authors do not present any power density or weight comparison in their results.

The rationale of this paper is to compare the effect of two core material options, namely low-loss 6.5% Si-Steel and Co-Iron steel on the performance and weight of the overall machine design. Initially, the material properties such as the B-H characteristics and losses at different frequencies are obtained with an experiment and then these material data are used to predict the performance of the machine designs using finite element simulations. The effect of stack length, number of winding turns, outer diameter and no-load magnetic flux density of the machine on the performance are compared. It is shown that the machines designed with Si-Steel at high core flux density are considerably lower in weight and achieves lower core losses than the Co-Iron designs. It is also shown that that the Co-Iron designs result in high core-losses that outweigh the higher copper-loss penalty encountered in the Si-Steel based designs. The performance of the designed machines are found to depend heavily on material selection and the operating point of the core. Therefore these need to be accounted in the design to improve power density.

Section II describes the target application and specific requirements associated with this application. Section III presents the experimental evaluation of the properties of the candidate material used for the comparison in this paper. Section IV details the machine design procedure specifically adopted to cater for the high speed operational requirements and for the comparison of the machine designs. Section V discusses the influence of the two different material on the machine performance and provides key conclusions. Section VI concludes the paper.

II. Target Application

The target application of this research is an aircraft starter generator. In contrast with the existing aero-engine generator technology, a starter-generator performs both the tasks of aircraft starter operation as well as power generation during flight. The starter operation is of short-time duty, while the power generation mode requires in continuous duty operation. Due operation in dual modes, a considerable weight saving is predicted by future more-electric aircraft engine designs.

For the starter/generator considered in this research, a nominal power of 45 kW at 32000 rpm is required. Fig. 1 shows the torque (magnitude) vs. speed requirement of the starter generator. The machine runs as a motor during engine start and is required to supply constant positive torque of approximately 54 Nm (T_{start}) from standstill to 8000 rpm (ω_{start}). Between ω_{start} to ω_{min} the machine provides a constant power to accelerate the engine until the engine is fired and achieves self-sustenance. When the machine reaches

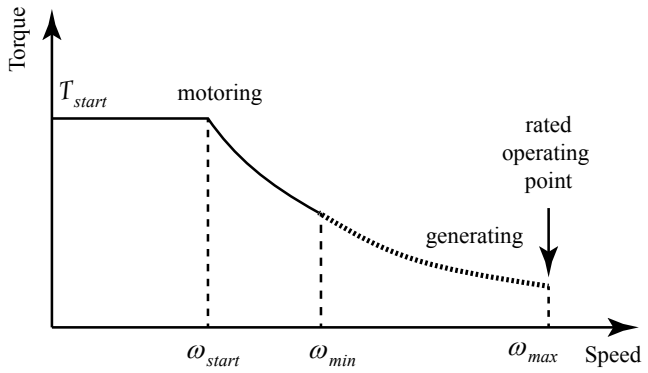

Fig. 1. Torque-Speed requirement of the aircraft starter-generator

ω_{min} the engine is considered to have achieved self-sustenance and generator operation is initiated. In generation mode, the machine is required to produce maximum constant power of 45 kW up to a maximum speed (ω_{max}) of 32000 rpm.

III. Experimental Evaluation of Material Properties

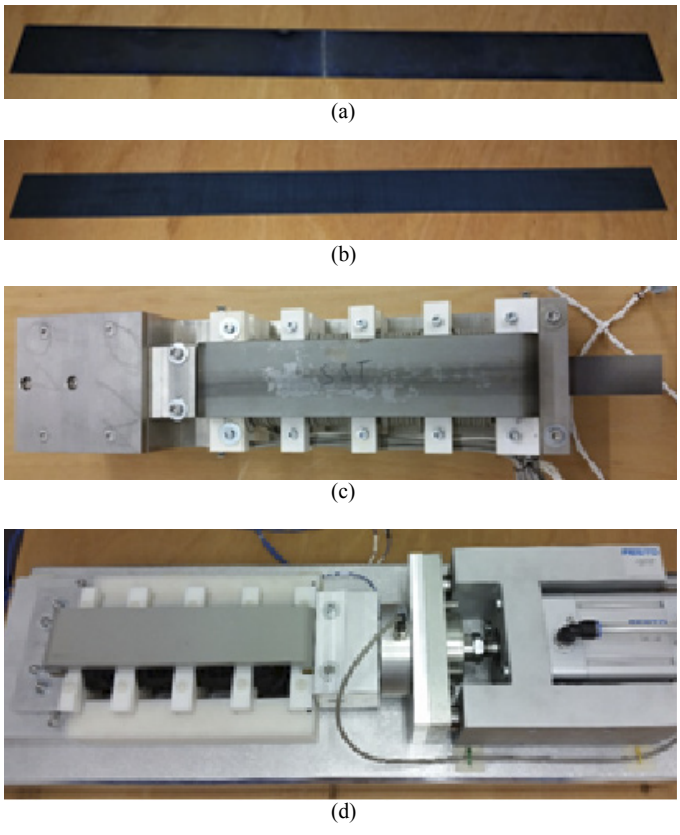

Fig. 2. Prepared material samples for testing: (a) Si-Steel sample and (b) Co-Iron alloy steel sample. (c) and (d) : Setup with the sample placed inside the testing unit during an experiment.

Due to the nature of the application, the machine operates continuously in high speed range and hence the reduction of the high frequency losses is a key requirement in the machine

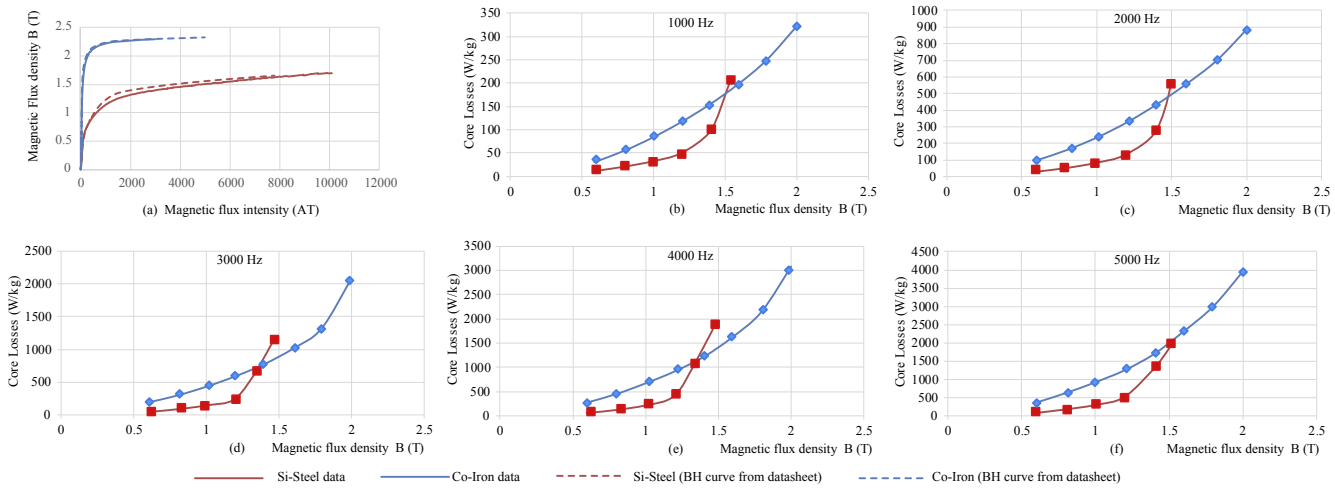

Fig. 3. (a) B-H characteristics and loss comparison of the two candidate materials - Silicon Steel and Cobalt-Alloy steel at different frequencies: (a) 1000 Hz, (b) 2000 Hz, (c) 3000 Hz, (d) 4000 Hz and (e) 5000 Hz.

design process. In addition, high power density is also a key criterion of the machine design. To achieve both high power density and high efficiency within the design, the selection of the material and its utilisation are important. Herein, two materials namely Co-Iron and 6.5% Si-Steel are considered for the design. The Co-Iron has significantly higher saturation flux density than Si-Steel as shown in Fig. 3 (a). However, Si-Steel has lower W/kg losses against frequency under normal operation. To perform an effective design, the properties of the materials are initially evaluated via an experiment and then integrated within Finite Element (FE) numerical tool.

The in-house material characterisation experimental setup uses three different methods to evaluate the core losses. The methods are the Epstein frame, single sheet tester and toroid core measurement methods. In this experiment, the both the Epstein frame based tests and single sheet tests have been performed. An example of the samples used for the tests are shown in Fig. 2 (a) and (b). The sampled being tested in the single sheet testing setup is shown in Fig. 2 (c) and (d).

TABLE I
SPECIFICATIONS AND CAPABILITIES FOR MEASUREMENT FACILITY

Parameter	Quantity
Fundamental Frequency	5 to 100 kHz
Low Frequency Amplifier Capacity (up to 20kHz - fundamental excitation)	100V 52 A (Peak) 60V 40A,(Continuous)
High Frequency Amplifier Capacity (up to 100kHz - nonsinusoidal / PWM)	50V 10A (peak & continuous)
Operating temperature: Soft Magnetic Materials Hard Magnetic Materials	-40C to 180C -40C to 300C
Operating stress (compression): Soft Magnetic Materials Hard Magnetic Materials	0 to 3kN 0 to 1kN
Excitation waveform capability:	Sine Wave, DC / Normalized, PWM, Harmonic injection

Fig. 4 shows the main interface of the measurement system that includes the power amplifier, measurement options, debugging options, heating unit, flux meter connections, real

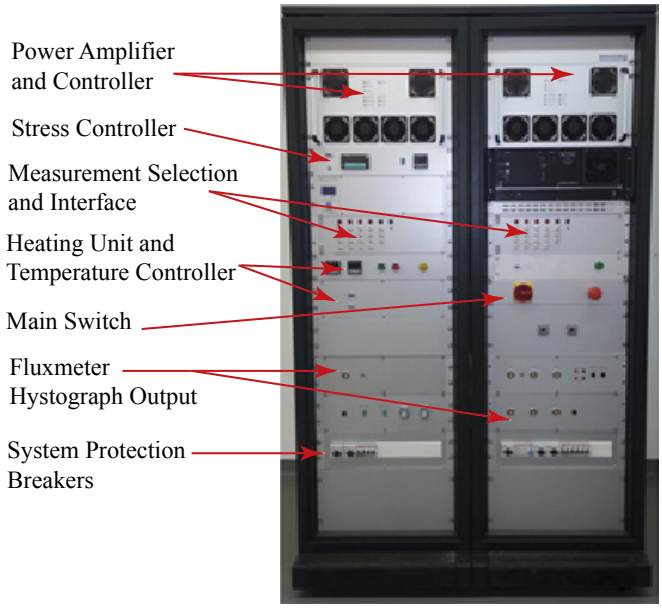

Fig. 4. Main interface of the state of art testing facility available in-house

time computer interface, and system protection arrangements. The setup specifications are shown in Table I. The power measurement is performed using a high fidelity system which consists of a linear power amplifier with high bandwidth and is IEC 60404 certified. The test samples are cut in standard geometry and tested according to specifications of the IEC 60404 standard. Device calibration has been performed with sinusoidal excitation and the form factor has been tightly governed in these tests. The final data has been gathered from several repetitive tests. The facility also provides the ability to perform the characterisation tests at any desired temperature and pressure depending on the furnace capability. Tests under multiple pressure and temperature values has not been considered in this study.

The commonly used watt-meter method is adopted in these

experiments for estimation of losses. Loss measurements at high magnetic flux density and high frequency have been possible with the single sheet tests. All the measurements are performed under pure sine wave excitation. The primary current and secondary voltage is then recorded. The complete hysteresis curve is generated using these two quantities and the B-H curves are obtained. The total iron losses are obtained by the high fidelity power measurement system presented in Table I. The copper losses are then subtracted. A temperature compensation is also provided to make sure that any change in resistance is compensated. The hysteresis losses are calculated by the area under the B-H curve. The remainder of the losses are assumed to be the eddy current and excess losses.

From Fig. 3 (a), it can clearly be seen that the measured B-H characteristics slightly varies from the data provided by the manufacturer due to variations during manufacture. However, they are in close agreement. It can also be seen from Fig. 3 (b) to (f) that as expected the losses increase with both flux density and frequency. The Si-Steel losses are higher than Co-Iron losses in the saturated region. This gives an indication that the design may be highly influenced by the region of the B-H curve where the machine is designed to be operated. The design has therefore been carried out based on both the material options and their characteristics obtained though these experiments. This will be detailed in the following section.

IV. Machine design strategy

The procedure adopted for the design of the machines to satisfy the stipulated operating point conditions is outlined in Fig. 5. The design process involves specification of the core no-load flux density B_{core} and the maximum stator outer diameter OD_{max}. The stator back-iron thickness and the stator tooth widths are direct function of these two specifications. Hence the preliminary stator dimensions for a given rotor pole number and SPP (slot per pole per phase) value can be determined such that the specified requirements are met. Dimensions such as slot opening and slot wedge thicknesses are maintained such that the tooth-edge flux density under no-load conditions remains the same as that of the tooth flux density, and hence offers a fair comparison in the analysis of the different designs. The rotor is designed with consideration on mechanical integrity and to achieve the highest power density within the given space-envelope for the machine [5]. The stator design is performed considering a bore diameter of 92 mm, air-gap thickness of 2 mm, magnet retention sleeve thickness of 4 mm and magnet thickness of 10 mm.

Based on the stator structure and the fixed rotor construction, the inductance and flux-linkage per-unit stack-length and unit winding-turns denoted by $\hat{L}$ and $\hat{\lambda}_{pm}$ are calculated. Simultaneously, the machine design is implemented in an FE package and the stator core maximum flux density and the FE based values of $\hat{L}$ and $\hat{\lambda}_{pm}$ are also evaluated. Following the matched $\hat{L}$ and $\hat{\lambda}_{pm}$, the feasible stack length and number of turns per winding are calculated. A feasibility machine design represents a machine with ability to satisfy maximum current limitation of 360 A, maximum voltage limitation of 270 V during both starting and field weakening operations. It is found that for a given rotor pole number and SPP combination, multiple feasible solutions exist. The different feasible machine design under different parametric variations are obtained as shown in Tables II (a) to (c) and are discussed in the following section.

V. Influence of the material on design

In this section, the variation of stack-length l_{stk} between 50 mm to 100 mm and outer diameter OD between 155 mm to 185 mm, and B_{core} value between 50% to 125% of the B_{max} value are investigated. From Fig. 3, the nominal maximum flux density B_{max} values are selected as 1.25 T and 2.05 T for Si-Steel and Co-Iron respectively.

These ranges of values are selected in this analysis to allow for an appreciable comparison of the variations of these parameters on the machine designs and their performance with the use of the two core material. The B_{core} value is specifically varied between 50% to 75% to capture the percentage improvement in power density and efficiency in the non-saturated region, and to 125% to capture the performance in the saturated region.

Fig. 6 outlines the 2-dimensional parameters, namely stator outer diameter OD, tooth width w_t, back-iron height w_b and tooth height h and their dependency on other parameters as explained in Section IV. The analysis is performed in three parts. Tables II (a), (b) and (c) outline the different versions

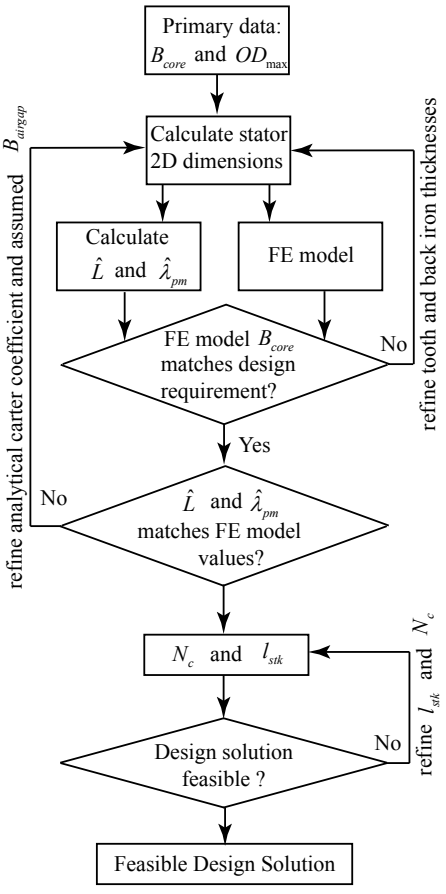

Fig. 5. The design process

TABLE II
THE DIFFERENT FEASIBLE MACHINE DESIGNS OBTAINED UNDER DIFFERENT PARAMETRIC VARIATIONS

Table (a) - Machine versions for the analysis of the effects of stack-length variation:
(designed with a outer diameter of 165 mm and a no-load maximum core magnetic flux-density of 75% of saturation flux-density of steel material)

Q	Ns	Design Version - Si-steel	stack length [mm]	Design Version - Co-Iron	stack length [mm]
12	14	A1	70.5	B1	74
12	12	A2	82.2	B2	86.4
24	6	A3	74.6	B3	76.2
24	5	A4	89.5	B4	91.4
18	11	A5	60.8	B5	62.3
18	10	A6	66.9	B6	68.5
18	9	A7	74.3	B7	76.1
18	8	A8	83.5	B8	85.6
36	6	A9	52	B9	50.9
36	5	A10	59.6	B10	61
36	4	A11	74.5	B11	76.3
36	3	A12	99.3	B12	101.7
24	6	A13	86.4	B13	88.6
24	7	A14	74	B14	76
24	8	A15	67.5	B15	66.5
48	3	A16	78.5	B16	79.3
48	4	A17	58.9	B17	59.5

4-pole designs
6-pole designs
8-pole designs

Table (b) - Machine variations for the analysis of the effects of outer diamater variation:
(designed with a selected stack-length and Ns values and a no-load maximum core magnetic flux-density of 75% of saturation flux-density of steel material.

Q	Ns	Outer diameter [mm]	Design Version - Si-steel	stack length [mm]	Design Version - Co-Iron	stack length [mm]
12	14	155	C1	70.5	D1	74
12	14	165	C2	70.5	D2	74
12	14	175	C3	70.5	D3	74
12	14	185	C4	70.5	D4	74
24	6	155	C5	74.6	D5	76.2
24	6	165	C6	74.6	D6	76.2
24	6	175	C7	74.6	D7	76.2
24	6	185	C8	74.6	D8	76.2
18	9	155	C9	74.3	D9	76.1
18	9	165	C10	74.3	D10	76.1
18	9	175	C11	74.3	D11	76.1
18	9	185	C12	74.3	D12	76.1
36	4	155	C13	74.5	D13	76.3
36	4	165	C14	74.5	D14	76.3
36	4	175	C15	74.5	D15	76.3
36	4	185	C16	74.5	D16	76.3
24	7	155	C17	74	D17	76
24	7	165	C18	74	D18	76
24	7	175	C19	74	D19	76
24	7	185	C20	74	D20	76
48	3	155	C21	78.5	D21	79.3
48	3	165	C22	78.5	D22	79.3
48	3	175	C23	78.5	D23	79.3
48	3	185	C24	78.5	D24	79.3

Table (c) - Machine variations for the analysis of the effects of no-load flux density variation: (designed with a selected stack-length and Ns values. Design varied with no-load maximum core magnetic flux-density from 50% to 125% of Bmax of steel material.

Q	Ns	% core flux density of B_{max}	Design Version - Si-Iron	stack length [mm]	Design Version - Co-steel	stack length [mm]
12	14	50	E1	70.5	F1	74
12	14	75	E2	70.5	F2	74
12	14	100	E3	70.5	F3	74
12	14	125	E4	70.5	F4	74
24	6	50	E5	74.6	F5	76.2
24	6	75	E6	74.6	F6	76.2
24	6	100	E7	74.6	F7	76.2
24	6	125	E8	74.6	F8	76.2
18	9	50	E9	74.3	F9	76.1
18	9	75	E10	74.3	F10	76.1
18	9	100	E11	74.3	F11	76.1
18	9	125	E12	74.3	F12	76.1
36	4	50	E13	74.5	F13	76.3
36	4	75	E14	74.5	F14	76.3
36	4	100	E15	74.5	F15	76.3
36	4	125	E16	74.5	F16	76.3
24	7	50	E17	74.0	F17	76
24	7	75	E18	74.0	F18	76
24	7	100	E19	74.0	F19	76
24	7	125	E20	74.0	F20	76
48	3	50	E21	78.5	F21	79.3
48	3	75	E22	78.5	F22	79.3
48	3	100	E23	78.5	F23	79.3
48	3	125	E24	78.5	F24	79.3

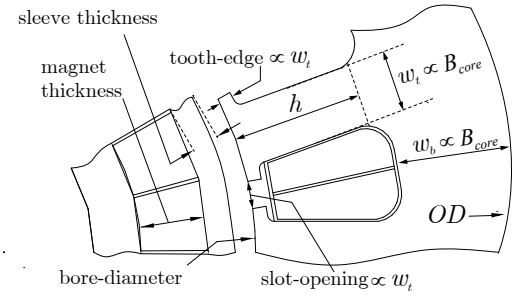

Fig. 6. Outline of a machine section with dimensions and the parameters that influence their selection

of feasible machine designs considered in the analysis.

Part-1: OD is fixed at 165 mm and B_{core} at 75% B_{max} of the corresponding material. l_{stk} and turns-per-slot N_s are varied. Resultant feasible designs are given in Table II (a).
Part-2 : OD is varied from 155 mm to 185 mm. B_{core} is fixed at 75% B_{max} of the corresponding material. l_{stk} and N_s are varied. Resultant feasible designs are given in Table II (b).
Part-3 : OD is fixed at 165 mm. B_{core} is varied from 50% B_max to 125% B_{max} of the corresponding material. l_{stk} and N_s are varied. Resultant feasible designs are given in Table II (c).

The 4-pole, 6-pole and 8-pole rotor options are considered and are highlighted in Tables II (a), (b) and (c) in different shades. These machine designs are obtained according to the procedure outlined in Section IV. For each slot-pole combination, the Si-steel designs and Co-steel designs achieve moderately close values of stack-length. However, the variation of the stack length is due to the difference in tooth thickness and material permeability in each design that result in a slight difference in stack-length requirement to satisfy the stipulated torque-speed requirements.

In this study, only double layer winding designs are investigated due to its lower winding harmonics. The Si-Steel machines are denoted by A- C- and E-, and Co-Iron machines are denoted by B-, D- and F- points as shown in Tables II (a), (b) and (c). The breakdown of losses, namely the steel core losses, eddy current losses in the magnets and the copper losses in the windings are obtained via FE simulations and the efficiencies at the rated operating point at a speed of 32000 rpm and output power of 45 kW is calculated. The machine weight and efficiency results are summarised in Fig. 7, 8 and 9.

A. Part - 1 : Variation of stack length and number of turns

The following are key observations from this analysis:

1) The efficiency variation with the increase in stack length is in the range of 1% for majority of the machines.

An example of this with the 6-pole / 36-slot machine designs is highlighted by lines L1 to L4 and the breakdown of loss components are shown in Table III. With higher stack-lengths, a higher field weakening current requirement yields higher copper losses. However, the maximum copper losses at starting is reduced as stack-length is increased due to resultant higher PM flux-linkage achieved. Hence, the change in efficiency is low.

2) The Co-Iron machine designs are found to be heavier than the Si-Steel machine designs.

For example, the breakdown of weights for the pair A10-B10 indicated by L2 is shown in Table IV. One of the main contributions to the weight is by the end-windings. The lower

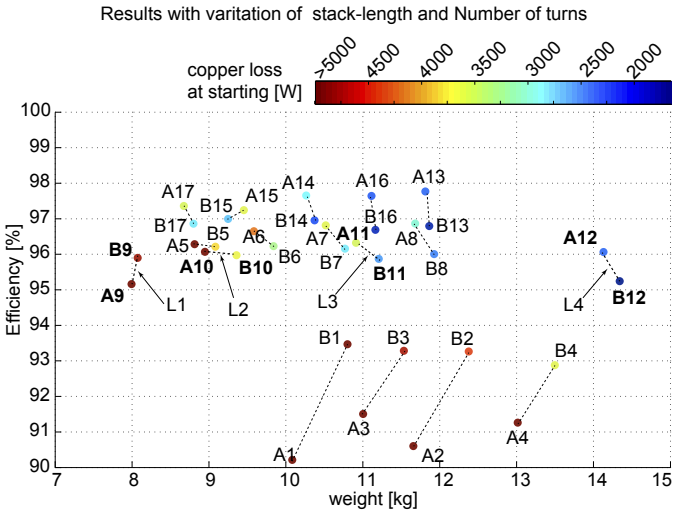

Fig. 7. Variation of efficiency and weight for feasible machine solutions for different stack length and number of turns per slot with fixed outer diameter at 165 mm and fixed no-load core flux density at 75% of B_{max} (Design versions A- are with Si-Steel and B- are with Co-Iron material)

TABLE III
BREAKDOWN OF LOSS COMPONENTS FOR THE 6-POLE, 36-SLOT MACHINE DESIGNS WITH VARIED l_{stk} AND N_s

XX	Copper loss [W]	Core loss [W]	Eddy current loss [W]	Total loss [W]	η %	Weight* [kg]
A9	2263.2	58.3	18.1	2339.5	95.2	7.99
A10	1762.5	72.3	15.2	1850.0	96.1	8.98
A11	1650.5	88.4	16.1	1755.0	96.3	10.91
A12	1753.0	112.2	19.7	1884.8	96.1	14.13
B9	1623.5	338.9	4.7	1967.2	95.9	8.07
B10	1466.1	411.5	4.8	1882.4	96.1	9.32
B11	1477.5	497.8	5.5	1980.8	95.9	11.21
B12	1662.4	627.8	7.1	2297.4	95.2	14.34

η - efficiency, * - weight only of active portion of the machine

stator weight with Co-Iron is outweighed by the higher copper weight.

B. Part - 2 : Variation of outer diameter / split ratio

This analysis is performed by varying the outer diameter from 155 mm to 185 mm over four steps. The split ratio is defined as:

$$\text{split ratio} = \frac{\text{inner diamater}}{\text{outer diamater}} \quad (1)$$

This variation in outer diameter corresponds to split ratios of 0.5935, 0.5576, 0.5257 and 0.4973 respectively. For each rotor pole and SPP combination, the tooth thickness and back-iron thickness hence remains the same. The increase in the outer diameter results in a higher tooth height and more area for the copper winding at the cost of a heavier machine. The following are key observations from this analysis:

1) The change in the outer diameter has minimal effect on the PM-flux linkage for each slot and SPP combination.

As a result, the machines with the same rotor pole number and SPP combination yield feasible machine solutions with approximately the same stack length. However, the increase in

TABLE IV
BREAKDOWN OF WEIGHTS OF DIFFERENT COMPONENTS OF THE MACHINE DESIGN FOR TWO 6-POLE 36-SLOT DESIGN VERSIONS - l_{stk} VARIATION

XX	Stator [kg]	Rotor [kg]	Magnet [kg]	Sleeve [kg]	Copper (main)	Copper (end)	Total* [kg]
A10	4.53	1.09	1.09	0.12	0.90	1.24	8.98
B10	3.86	1.12	1.12	0.12	1.31	1.79	9.32

* - weight only of active portion of the machine

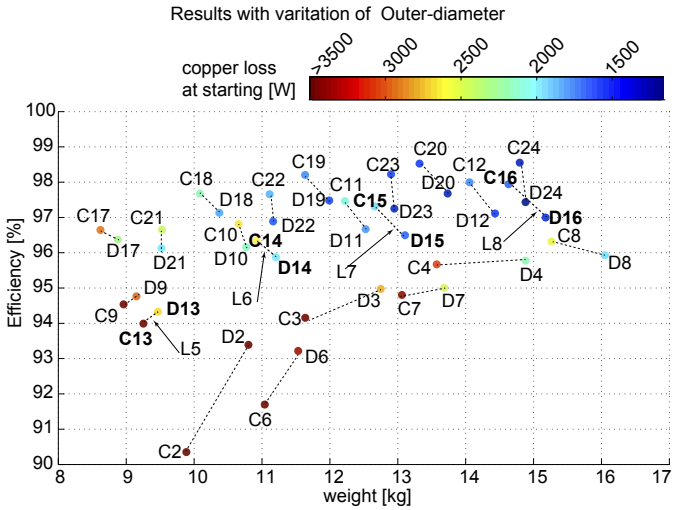

Fig. 8. Variation of efficiency and weight for feasible machine solutions for different outer diameter (155 mm, 165 mm 175 mm and 185 mm) for feasible machine designs with stack length between 70 mm to 80mm and fixed no-load core flux density at 75% of Bmax. Design versions C- are with Si-Steel and D- are with Co-Iron material

the outer diameter results in a higher inductance that translate to a lower current requirement at the field weakening operating point at 32000 rpm. Furthermore, increase in outer diameter also result in more area for copper and lower copper losses. This results in an added increase in efficiency at the cost of a heavier machine.

An example with C13 to C16 for the Si-Steel machines and D13 to D16 for the Co-Iron machines is given in Table V. The reduction in split ratio from 0.5935 to 0.5576 results in an increase in efficiency by 2.3% and 1.6% for the Si-Steel machines and Co-Iron machines respectively. The reduction in split ratio from 0.5935 to 0.4973 results in a total increase of in efficiency of 3.9% and 2.7% for the Si-Steel machines and Co-Iron machines respectively.

2) As the outer diameter is increased (split ratio is reduced), the difference between the weights of the Si-Steel machines and the Co-Iron machines further expand.

This is mainly due to the higher copper weight in the Co-Iron design especially contributed by the end-windings. An example with C13 to C16 for the Si-Steel machines and D13 to D16 for the Co-Iron machines is given in Table VI. The reduction in split ratio from 0.5935 to 0.5576 results in an increase in weight by 1.66 kg and 1.74 kg for the Si-Steel machine and Co-Iron machines respectively. The reduction in split ratio from 0.5935 to 0.4973 results in a total increase of in weight of 1.97 kg and 2.07 kg for the Si-Steel machine and

TABLE V
BREAKDOWN OF LOSS COMPONENTS FOR THE 6-POLE, 36-SLOT MACHINE DESIGNS WITH VARIED OD

XX	Copper loss [W]	Core loss [W]	Eddy current loss [W]	Total loss [W]	Core loss% out of total loss	η %
C13	2855.9	79.1	5.5	2940.5	2.7	94.0
C14	1650.5	88.4	5.2	1744.1	5.1	96.3
C15	1171.4	94.3	5.3	1270.9	7.4	97.3
C16	858.6	104.4	5.2	968.1	10.8	97.9
D13	2297.6	457.1	11.4	2766.0	16.5	94.3
D14	1477.5	497.8	5.5	1980.8	25.1	95.9
D15	1047.7	569.0	5.3	1621.9	35.1	96.6
D16	789.7	627.8	5.4	1422.9	44.1	97.0

split ratios : C13 & D13 - 0.5935, C14 & D14 - 0.5576
C15 & D15 - 0.5257 and C16 & D16 - 0.4973
η - efficiency

TABLE VI
BREAKDOWN OF WEIGHTS OF DIFFERENT COMPONENTS OF THE MACHINE DESIGN FOR 6-POLE 36-SLOT DESIGN VERSIONS - SPLIT RATIO VARIATION

XX	Stator [kg]	Rotor [kg]	Magnet [kg]	Sleeve [kg]	Copper (main)	Copper (end)	Total [kg]
C13	4.89	1.36	1.37	0.14	0.72	0.77	9.25
D13	4.26	1.40	1.40	0.15	1.10	1.16	9.47
C14	5.59	1.36	1.37	0.14	1.17	1.29	10.92
D14	4.83	1.40	1.40	0.15	1.64	1.79	11.21
C15	6.29	1.36	1.37	0.14	1.66	1.91	12.74
D15	5.41	1.40	1.40	0.15	2.22	2.54	13.11
C16	6.96	1.36	1.37	0.14	2.19	2.61	14.63
D16	5.98	1.40	1.40	0.15	2.86	3.40	15.18

Co-Iron machines respectively.

C. Part - 3 : Variation of design no-load core flux density

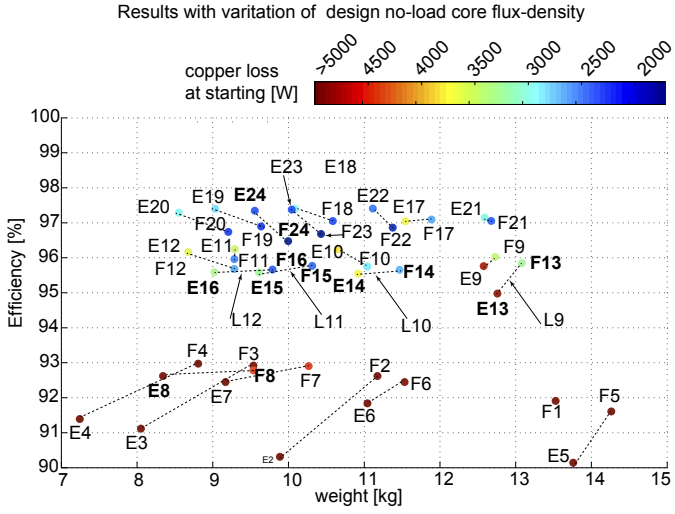

Fig. 9. Variation of efficiency and weight for feasible machine solutions for different no-load flux density selections (50%, 75%, 100% and 125% of Bmax) for feasible machine designs with stack length between 70 mm to 80mm and outer diameter of 165mm. Design versions E- are with Si-Steel and F- are with Co-Iron core material.

Both the earlier analyses have been performed on machines designed with a no-load core flux density B_{core} at 75% of the nominal maximum flux density B_{max}. In this section, the B_{core} is varied from 50%, 75% 100% and 125% of B_{max} respectively. The 125% case represents the design of a machine in the saturated region and hence the effects of saturation on the field-weakening operating point are accommodated in the analysis.

Based on the results in Fig. 9, the following key observations are made:

1) As the pole number increases, higher efficiency is observed.

TABLE VII
BREAKDOWN OF LOSS COMPONENTS FOR THE 4-POLE, 6-POLE AND 8-POLE, 2-SPP MACHINE DESIGNS WITH B_{core} AT 125% OF B_{max}

XX	pole-pairs	Copper loss [W]	Core loss [W]	Eddy current loss [W]	Total out of	η %
E8	4	3448.0	97.4	119.7	3665.1	92.6
E16	6	1971.8	137.1	13.8	2122.6	95.6
E24	8	1104.8	120.1	30.7	1255.6	97.3
F8	4	2865.6	519.4	141.7	3526.6	92.9
F16	6	1335.8	739.0	10.0	2084.8	95.7
F24	8	859.4	781.7	38.2	1679.3	96.5

As the pole number increases, higher efficiency is observed for all variations of B_{core} values. As an example, Table VII shows the variation of efficiency and losses with incremented pole-pair numbers for both the Si-Steel and Co-Iron designs. With higher pole-pair number, the back-iron requirement is reduced, and hence more area for copper is available. This results in lower copper losses in the 8-pole machine designs resulting in an improvement in efficiency.

2) As the B_{core} value is increased, the relative difference in weight between the Si-Steel and Co-Iron machines widens.

TABLE VIII
BREAKDOWN OF WEIGHTS OF DIFFERENT COMPONENTS OF THE MACHINE DESIGN FOR 6-POLE 36-SLOT DESIGN VERSIONS - B_{core} VARIATION

XX	Stator [kg]	Rotor [kg]	Magnet [kg]	Sleeve [kg]	Copper (main)	Copper (end)	Total [kg]
E13	8.03	1.36	1.37	0.14	0.88	0.98	12.76
E14	5.20	1.36	1.37	0.14	1.21	1.34	10.62
E15	3.84	1.36	1.37	0.14	1.38	1.52	9.61
E16	3.04	1.36	1.37	0.14	1.48	1.62	9.02
F13	7.43	1.40	1.40	0.15	1.29	1.42	13.08
F14	5.20	1.40	1.40	0.15	1.59	1.74	11.47
F15	5.20	1.40	1.40	0.15	1.59	1.74	11.47
F16	2.84	1.40	1.40	0.15	1.91	2.09	9.79

This observation follows a similar argument to that observed with the variation of outer diameter. An example with breakdown of weights for the 6-pole / 36-slot machines are shown in Table VIII and is also highlighted in Fig. 9 by the lines represented by L9, L10, L11 and L12. This can be mainly attributed to the heavier windings in the Co-Iron machines. Also it is worth noting that the reduction in weight from the design of the machines with B_{core} of 50% B_{max} to a B_{core} of 125% B_{max} is at 3.74 kg and 3.3 kg for the Si-Steel and Co-Iron machines respectively.

D. The following are key general observations are also obtained from the analysis:

1) The 4-pole machines generally under-perform in comparison with the remaining machine designs.

Overall the efficiency of the 4-pole machines is below 94% for majority of the 4-pole machines and the copper losses at the 8000 rpm starting condition is above 3.5 kW. Hence the 4-pole machines can be considered as unsuitable for this application.

2) Compared with the Co-Iron machines, Si-Steel machines yield higher copper losses.

This is mainly due to the lower area for the copper winding in the Si-Steel machine designs. However, the reduction in core losses in the Si-Steel for this particular machine design is found to outweigh the copper losses for majority of the 6-pole and 8-pole machine designs. Hence as observed in Figs. 7 to 9 for a large cohort of 6-pole and 8-pole machines, higher efficiency is achieved by the Si-Steel machines with a reduction in weight by at least 3.8% for the 6-pole machines and 1.4% for the 8-pole machines compared to Co-Iron machine.

The 8-pole machines offer superior overall performance over efficiency and weight. However, evaluation of power electronic and drive system efficiency reveal that the power electronic converter may be compromised with higher losses due to high power frequency. Hence, the prototype selection is based on the 6-pole machine options. Based on the analysis performed, it can be deduced that the best option is Si-Steel due to the lower weight offered and the comparatively low cost of material. The copper losses at starting is limited below 3.5 kW due to cooling limitations. Furthermore, with allowance for the machine casing and cooling space, the outer diameter of 165 mm is selected and the machine option of 6-pole 36-slot design is selected and designed for a no-load flux density of 75% B_{max}.

VI. Conclusion

The effect of two soft magnetic materials, namely Si-Steel and Co-Iron on the machine design has been investigated. The material properties of these two candidate Steels have been experimentally evaluated and their B-H characteristics and the core losses have been obtained. Based on this information, an aircraft starter-generator design is considered. The variation of the stack-length and number of winding turns, the outer diameter of the machine and the variation of the design core flux density have been investigated. The key observations can be summarised as:

1. Increase in slot area/copper area in Co-Iron machines reduces the core steel weight. However, this increases the overall machine weight due to higher copper volume especially due to the end-windings. Although the copper losses are reduced due to increase in copper volume, in majority of the machines the increase coreless outweighs the reduction in copper loss in comparison with Si-Steel machines.

2. There is no significant advantage on efficiency (at rated operating point) by increase of stack length and number of turns due to increase in field weakening requirement. The change in efficiency is found to be within 1%. However, the changes in stack length are found to impact the copper losses incurred at the starting condition.

3. For different stack-length and number of turn combinations, the reduction in copper losses from a Si-Steel design to a Co-Iron design for 6-pole and 8-pole machine designs is found to be in the range of 5% to 28% for an increase in overall weight in the range of 0.05 kg to 0.7 kg.

4. A reduction in split ratio from 0.5935 to 0.5576 has shown an increase in efficiency by 2.3% and 1.6% for the Si-Steel machines and Co-Iron machines respectively. This is for an increase in weight by 1.66 kg and 1.74 kg respectively. Similarly, the reduction in split ratio from 0.5935 to 0.4973 has shown an increase of in efficiency of 3.95% and 2.67% for the Si-Steel machine and Co-Iron machines respectively. This is for an increase in weight by 1.97 kg and 2.07 kg respectively.

5. For the 6-pole/36 slot case, the increase in flux density from 50% B_{max} to 125% B_{max} resulted in an increase in core losses by 3.6% for the Si-Steel machines and 15.8% for the Co-Iron machines, whilst reduction in the weight is 3.74 kg and 3.3 kg respectively. Similar trend has also been found in other slot/pole combinations.

In Conclusion, the Si-Steel machines appear to outperform the Co-Iron machines both in-terms of weight and efficiency for the application considered. Although Co-Iron material is more expensive than the Si-Steel material, there is no advantage of a machine designed with the more expensive material. This also confirms the fact that the machine design depends significantly on material selection and the operating point of the core. These need to be accounted for in the design to improve power density.

References

[1] Y. Jia and K. Rajashekara, "An induction generator based ac/dc hybrid electric power generation system for more electric aircraft," in *IEEE Industry Applications Society Annual Meeting, 2015*, Oct 2015, pp. 1–7.

[2] R. Bojoi, A. Cavagnino, A. Tenconi, and S. Vaschetto, "Control of shaft-line-embedded multiphase starter/generator for aero-engine," *IEEE Trans. Ind. Electron.*, vol. 63, no. 1, pp. 641–652, Jan 2016.

[3] D. Wu, R. Todd, and A. J. Forsyth, "Adaptive rate-limit control for energy storage systems," *IEEE Trans. Ind. Electron.*, vol. 62, no. 7, pp. 4231–4240, July 2015.

[4] E. Levi, "Advances in converter control and innovative exploitation of additional degrees of freedom for multiphase machines," *IEEE Trans. Ind. Electron.*, vol. 63, no. 1, pp. 433–448, Jan 2016.

[5] W. U. N. Fernando and C. Gerada, "High speed permanent magnet machine design with minimized stack-length under electromagnetic and mechanical constraints," *Int J Appl Electrom.*, vol. 46, no. 1, pp. 95–109, Jan 2014.

[6] A. Boglietti, C. Gerada, and A. Cavagnino, "High-speed electrical machines and drives [special section intro.]," *IEEE Trans. Ind. Electron.*, vol. 61, no. 6, pp. 2943–2945, June 2014.

[7] J. Boisson, F. Louf, J. Ojeda, X. Mininger, and M. Gabsi, "Analytical approach for mechanical resonance frequencies of high-speed machines," *IEEE Trans. Ind. Electron.*, vol. 61, no. 6, pp. 3081–3088, June 2014.

[8] A. Borisavljevic, H. Polinder, and J. A. Ferreira, "On the speed limits of permanent-magnet machines," *IEEE Trans. Ind. Electron.*, vol. 57, no. 1, pp. 220–227, Jan 2010.

[9] D. Gerada, A. Mebarki, N. L. Brown, K. J. Bradley, and C. Gerada, "Design aspects of high-speed high-power-density laminated-rotor induction machines," *IEEE Trans. Ind. Electron.*, vol. 58, no. 9, pp. 4039–4047, Sept 2011.

[10] D. Gerada, A. Mebarki, N. L. Brown, C. Gerada, A. Cavagnino, and A. Boglietti, "High-speed electrical machines: Technologies, trends, and developments," *IEEE Trans. Ind. Electron.*, vol. 61, no. 6, pp. 2946–2959, June 2014.

[11] A. Tenconi, S. Vaschetto, and A. Vigliani, "Electrical machines for high-speed applications: Design considerations and tradeoffs," *IEEE Trans. Ind. Electron.*, vol. 61, no. 6, pp. 3022–3029, June 2014.

[12] A. Tuysuz, C. Zwyssig, and J. W. Kolar, "A novel motor topology for high-speed micro-machining applications," *IEEE Trans. Ind. Electron.*, vol. 61, no. 6, pp. 2960–2968, June 2014.

[13] N. Uzhegov, E. Kurvinen, J. Nerg, J. Pyrhonen, J. T. Sopanen, and S. Shirinskii, "Multidisciplinary design process of a 6-slot 2-pole high-speed permanent-magnet synchronous machine," *IEEE Trans. Ind. Electron.*, vol. 63, no. 2, pp. 784–795, Feb 2016.

[14] A. Aigbomian, P. Arumugam, T. Hamiti, and C. Gerada, "Fast computing tool for performance evaluation in interior permanent magnet machines," in *Int. Conf. on Electrical Machines (ICEM)*, Sept 2014, pp. 2722–2727.

[15] P. Arumugam, T. Hamiti, and C. Gerada, "Estimation of eddy current loss in semi-closed slot vertical conductor permanent magnet synchronous machines considering eddy current reaction effect," *IEEE Trans. Magn.*, vol. 49, no. 10, pp. 5326–5335, Oct 2013.

[16] D. J. Powell, G. W. Jewell, S. D. Calverley, and D. Howe, "Iron loss in a modular rotor switched reluctance machine for the "more-electric" aero- engine," *IEEE Trans. Magn.*, vol. 41, no. 10, pp. 3934–3936, Oct 2005.

[17] S. P. Nikam and B. G. Fernandes, "Design of soft magnetic composite based modular four phase srm for electric vehicle application," in *Int. Conf. on Electrical Machines (ICEM)*, Sept 2014, pp. 112–116.

[18] D. Dorrell, L. Parsa, and I. Boldea, "Automotive electric motors, generators, and actuator drive systems with reduced or no permanent magnets and innovative design concepts," *IEEE Trans. Ind. Electron.*, vol. 61, no. 10, pp. 5693–5695, Oct 2014.

[19] L. Ferraris, P. Ferraris, E. Poskovic, and A. Tenconi, "Theoretic and experimental approach to the adoption of bonded magnets in fractional machines for automotive applications," *IEEE Trans. Ind. Electron.*, vol. 59, no. 5, pp. 2309–2318, May 2012.

[20] W. Zhao, T. A. Lipo, and B. il Kwon, "Material-efficient permanent-magnet shape for torque pulsation minimization in spm motors for automotive applications," *IEEE Trans. Ind. Electron.*, vol. 61, no. 10, pp. 5779–5787, Oct 2014.

[21] R. D. Stefano and F. Marignetti, "A comparison between soft magnetic cores for axial flux pm synchronous machines," in *Int. Conf. on Electrical Machines (ICEM)*, Sept 2012, pp. 1922–1927.

[22] R. H. Qu, "Keynote talk 2014 - design of large electrical machines," in *IEEE Int. Conf. on Applied Superconductivity and Electromagnetic Devices (ASEMD 2013)*, Oct 2013, pp. 536–536.

[23] W. Zhao, T. A. Lipo, and B. il Kwon, "Dual-stator two-phase permanent magnet machines with phase-group concentrated-coil windings for torque enhancement," *IEEE Trans. Magn.*, vol. 51, no. 11, pp. 1–4, Nov 2015.

[24] J. Ma, R. Qu, and J. Li, "A novel axial flux switched reluctance motor with grain oriented electrical steel," in *Magnetics Conference (INTERMAG), 2015 IEEE*, May 2015, pp. 1–1.

[25] R. Kolano, A. Kolano-Burian, K. Krykowski, J. Hetmanczyk, M. Hreczka, M. Polak, and J. Szynowski, "Amorphous soft magnetic core for the stator of the high-speed pmbldc motor with half-open slots," *IEEE Trans. Magn.*, vol. PP, no. 99, pp. 1–1, 2016.

[26] M. N. Ibrahim, P. Sergeant, and E. M. Rashad, "Synchronous reluctance motor performance based on different electrical steel grades," *IEEE Trans. Magn.*, vol. 51, no. 11, pp. 1–4, Nov 2015.

[27] Y. Zhang, Q. Li, Y. Wang, Z. Ren, J. Xia, and D. Xie, "Anisotropic magnetostriction of nonoriented silicon steel sheet and its frequency dependence," *IEEE Trans. Magn.*, vol. 51, no. 11, pp. 1–4, Nov 2015.

[28] A. Chiba, K. Kiyota, N. Hoshi, M. Takemoto, and S. Ogasawara, "Development of a rare-earth-free sr motor with high torque density for hybrid vehicles," *IEEE Trans. Energy Convers.*, vol. 30, no. 1, pp. 175–182, March 2015.

[29] W. U. N. Fernando and M. Barnes, "Electromagnetic energy conversion efficiency enhancement of switched reluctance motors with zero-voltage loop current commutation," *IEEE Trans. Energy Convers.*, vol. 28, no. 3, pp. 482–492, Sept 2013.

Nuwantha Fernando (M'10) received the B.Sc degree in Electrical Engineering from University of Moratuwa, Sri Lanka in 2008 and the Ph.D degree from the University of Manchester, U.K., in 2012. Subsequently he has been a researcher at the University of Nottingham and thereafter at University of Oxford. He is presently Lecturer at the RMIT University Melbourne. His research interests include electric machines and drives particularly for electric transportation applications.

Gaurang Vakil received the B.E. degree in electrical engineering from the Saurashtra University in 2006 and M. Tech. with Gold Medal from the Nirma University in 2008. He is currently working toward completion of the Ph.D. degree in variable speed generator design for renewable energy applications with the Power Electronics, Machines and Drives (PEMD) group at Indian Institute of Technology - Delhi (IITD). He is also working as a Research Associate with Power Electronics, Machines and Controls (PEMC) group at the University of Nottingham. His main research interests are analytical modelling and design optimization of electrical machines, optimizing electric drive-train for pure electric and hybrid vehicles, high power density machines, magnetic material characterization and high-performance electrical machines for transport, traction and renewable energy applications.

Puvan Arumugam (M'11) received the B.Eng. (Hons.) degree in electrical and electronic engineering from The University of Nottingham, Nottingham, U.K., in 2009, and the Ph.D. degree in electrical machines and drives from The University of Nottingham, Nottingham, U.K., in 2013. He subsequently worked as a researcher within the Power Electronics, Machines, and Control Group, The University of Nottingham, working on electric aircraft propulsion. He is currently a Senior Project Engineer with the Force Engineering Ltd, Shepshed, UK. His current research interests include electrical machines and drives, electromechanical devices and systems, and analytical computation of electromagnetic fields. Dr. Arumugam was awarded a Hermes Fellowship supported by Technology Transfer Office, The University of Nottingham in 2014.

Emmanuel Amankwah received the BSc degree in Electrical & Electronic Engineering from KNUST (2006), Ghana and the MSc and PhD degrees in Electrical engineering (2009) and Electrical & Electronic Engineering (2013), respectively, from The University of Nottingham, Nottingham, U.K. Between 2006 and 2008 Emmanuel worked with the Electricity Company of Ghana as a design Engineer. Since 2013, he has being working as a Research Fellow in emerging technologies for HVDC power transmission at the Power Electronic Machines and Control research group (PEMC) at the University of Nottingham, Faculty of Engineering, Nottingham. His main research activities are in power electronics for grid integration and has interest in motor drive control.

Chris Gerada (M'05) received the Ph.D. degree in numerical modeling of electrical machines from The University of Nottingham, Nottingham, U.K., in 2005. He subsequently worked as a Researcher with The University of Nottingham on high-performance electrical drives and on the design and modeling of electromagnetic actuators for aerospace applications. Since 2006, he has been the Project Manager of the GE Aviation Strategic Partnership. In 2008, he was appointed as a Lecturer in electrical machines; in 2011, as an Associate Professor; and in 2013, as a Professor at The University of Nottingham. His main research interests include the design and modeling of high-performance electric drives and machines. Prof. Gerada serves as an Associate Editor for the IEEE Transactions on Industry Applications and is the Chair of the IEEE IES Electrical Machines Committee.

Serhiy Bozhko (M'96) received the M.Sc. and Ph.D. degrees in electromechanical systems from the National Technical University of Ukraine, Kyiv city, Ukraine, in 1987 and 1994, respectively. Since 2000, he has been with the Power Electronics, Machines and Controls Research Group of the University of Nottingham, Nottingham, U.K. Serhiy has been a Principal Research Fellow and is currently an Associate Professor in Aircraft Electrical Systems. He has been involved in leading several EU- and industry-funded projects in the area of aircraft electric power systems, including control and stability issues, power management, as well as advanced modeling and simulations methods.